Controlling Femtosecond Laser Filaments via Quasi-Hermite Gaussian Beam Modes

N. Kaya[a,*], G. Kaya[b], A. Kolomenski[c] and H. Schuessler[c]

[a] *Department of Material Science and Engineering, Faculty of Engineering, Çanakkale Onsekiz Mart University, TR-17100 Çanakkale, Turkey*
[b] *Department of Electric and Energy, Canakkale Vocational School of Technical Sciences, Çanakkale Onsekiz Mart University, TR-17100 Çanakkale, Turkey*
[c] *Department of Physics & Astronomy, Faculty of Science, Texas A&M University, College Station, TX, 77843-4242, USA*

Received: 12.11.2021 & Accepted: 03.01.2022

Doi: 10.12693/APhysPolA.141.204 *e-mail: necatikaya@comu.edu.tr

We present the possibilities of controlling and organizing femtosecond laser filaments and white-light formation via generating quasi-Hermite Gaussian beam modes in water. The quasi-Hermite Gaussian modes are created as transverse structures with different intensity and phase distributions by modulating the spatial phase front in the incident Gaussian beam. We have created phase masks on a spatial light modulator to produce desired beam profiles such as quasi-Hermite Gaussian beam modes. By creating the quasi-Hermite Gaussian beam modes from the incident Gaussian mode, we have shown that multiple filaments and white-light generation patterns can be controlled and organized depending on the created beam mode profile. Since only one initial beam was employed, the beam and the created side patterns were mutually coherent, which enables their use for pump–probe spectroscopy and other experiments requiring mutual coherence of the beams employed.

topics: filamentation, beam modes, nonlinear optics

1. Introduction

Filamentation can appear as a result of the self-focusing of intense ultrashort pulses that is restrained by ionization of the medium [1, 2]. Filamenting pulses can propagate over long distances due to the sustaining dynamic energy balance in the filament structure. Accompanying nonlinear dynamic phenomena, such as strong spectral broadening [3–5] make filament generation an interesting research topic of nonlinear optics, related to the interaction of extreme ultrafast optical fields with matter, which finds various applications, such as remote sensing, high harmonic generation, etc. [6–11]. For these important applications, filaments must be produced reproducibly and in a well-organized and controlled fashion. Filament formation is the result of balancing the Kerr self-focusing of an intense laser pulse and defocusing by plasma generation and ionization of the medium [12–15]. Consequently, the intensity profile plays an important role in filamentation and resulting white-light supercontinuum generation. Small intensity irregularities on the laser beam profile can be efficiently enhanced through filament generation [16]. Such inhomogeneities in the transverse profile of a propagating pulse are always present due to inherent variations of the laser generation process and perturbations of the surface and medium in the path of the optical beam. Multiple filaments from such distortions would naturally occur, and in the case of the high input peak power, the generation of a multi-filament structure is normally unavoidable. In addition, different filaments in this structure randomly compete for energy distribution [16–19]. The so-called mature filament is the one that undergoes the self-focusing process and propagation and develops enhanced self-phase modulation resulting in spectral broadening, i.e, white-light continuum generation [16]. Often, competing filaments end prematurely [20], thus reducing related ionization and subsequent fluorescence of molecules due to suppressed molecular excitation and filamentation [17]. The inherent instability of filamentation calls for a practical solution allowing for systematic and reliable control of this process. A possible approach can be to impose a regular artificial perturbation in the path of the incident beam that creates a template for the development of the filament structure. For instance, highly reproducible

filamentation patterns in water were predetermined by introducing a small incident beam ellipticity [21]. The arranging of a regular filament formation in the air was demonstrated by applying phase distortions or gradients in the incident pulse [22]. Filament formation was also organized and controlled by redistributed laser intensity by applying a 180° phase step on a spatial light modulator (SLM) [23]. This induced diffraction, causing the exceeding of the critical threshold, which resulted in filament generation. By arranging the focusing of different spatial parts of the original beam, filaments were created in an arbitrary array in fused silica by using an SLM [24]. The control of multiple filaments was numerically studied by imposing a periodic mesh onto the beam profile with random intensity perturbations [25]. This periodic mesh creates a regular field variation in the beam profile, resulting in deterministic multi-filaments [26, 27]. By inserting diffractive optical elements into the path of an intense pulse from a Ti:sapphire laser system, stable one- and two-dimensional arrays of filaments were experimentally produced due to highly structured diffraction patterns [20]. The organization of regular filamenting patterns is also demonstrated in other studies by introducing field gradients, phase distortions, as well as by beam shaping [23, 28–31]. For the latter, a deformable mirror [22, 32, 33], a double lens set-up [34], or patterned optical fields [35] were used.

In this study, we generated quasi-Hermite Gaussian (HG) beam modes with specially realized phase masks on an SLM and used holographical flexibility instead of deterministic mechanical or optical elements, such as meshes, slits, apertures, etc. With this approach we created a regular spatially redistributed intensity of beam modes, such as quasi-HG profiles, to control femtosecond laser filaments and related white-light formation by causing the critical threshold for filament formation to be exceeded. We experimentally confirmed that multiple filaments and white-light supercontinuum generation can be actively organized and controlled by generated beam modes in a phase-only SLM. Since employment of an SLM provides a high degree of flexibility and can universally be applied to the generation of a variety of beam profiles, this method can be adapted to many practical applications requiring control and organization of femtosecond filaments and the white-light generation. Our findings show that HG beam modes can efficiently control the structure of filamentation and can therefore be implemented in many nonlinear optics applications. An important property of multiple filaments produced from one incident beam is that the light in these filaments is mutually coherent. The coherence of the white-light continuum from such multiple filaments was studied and verified in [36], and this property can be used for pump-probe spectroscopy and other experiments, where the mutual coherence of the employed beams is a prerequisite.

2. Experimental procedures, results, and discussion

The experimental layout is depicted in Fig. 1a. We employed laser pulses emitted from a 1 kHz Ti:sapphire laser system having 50 fs pulse duration, 800 nm central wavelength, and 1 mJ per pulse output energy. The experimentally created beam modes were sent into a glass cell filled with water. The beam profiles were imaged onto CCD (Mightex, 1.4MP 1/2" CCD) monochrome and color cameras placed with proper filters at the exit of the beam.

To create quasi-HG beam modes, we modified the spatial phase distribution of an initial Gaussian beam. The respective phase masks imposed on the SLM (Hamamatsu LCOS-SLM 104683) are shown in the inset of Fig. 1a. In the phase distributions shown, the pixels for which the phase shift is 0 are rendered black, and the ones with the phase shift equal to π are shown as white. The SLM phase modulation was factory calibrated and produced phase modulation in excess of 2π radians at 800 nm. We applied a phase-only modification to the incident Gaussian beam from the laser system. As a result, the resulting beam was a superposition of HG beams with different mode numbers — we call them quasi-HG modes. These quasi-HG beams have side lobes as presented in Fig. 2a–d.

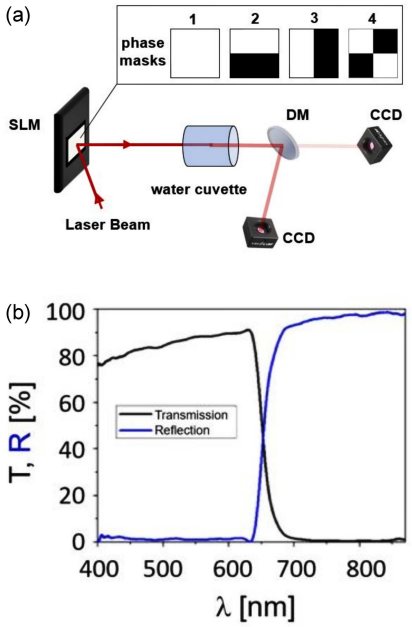

Fig. 1. (a) Experimental layout. In the inset, the phase distributions are given to generate quasi-HG beams on the SLM, where pixels with 0-phase are rendered black and the ones with π-phase are shown as white. The dielectric mirror (DM) was used to separate the IR radiation from the laser source and the generated white-light. (b) The transmission T and reflection R are shown in the graph on the right. The separated radiations were imaged on the CCD cameras.

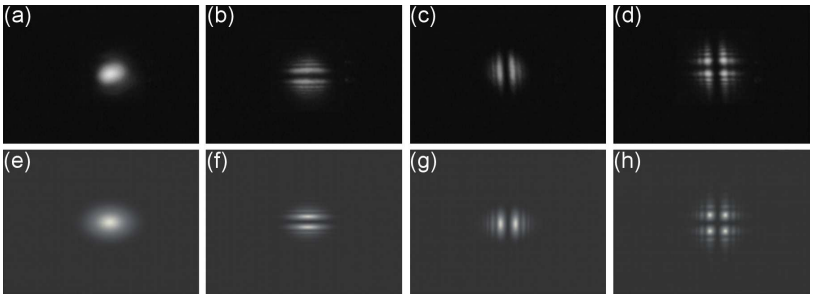

Fig. 2. (a–d) The measured laser intensity distributions of the quasi-HG beams with the phase masks (1–4) from the inset of Fig. 1 (e–h) The intensity distributions calculated with the diffraction integral of (1) for the same phase masks.

The intensity distributions for quasi-HG beams were calculated as described in [37, 38]. The incident beam was assumed to be Gaussian (HG_{00} mode) $E(x', y', z = 0) = E_0 \, \mathrm{e}^{-(x'^2+y'^2)/w_0^2}$ with the radius of the beam w_0 on the SLM. From the full width $\Delta x_{\mathrm{FW}} \, \mathrm{e}^{-1} = w_0\sqrt{2} = 1.16$ mm at the e^{-1} level of the beam intensity distribution, the beam radius w_0 is determined to be $w_0 = 0.82$ mm. The images of the distribution of the laser intensity in HG beams were recorded by using a CCD camera with sensor size 7.60×6.20 mm^2 at the distance $L = 70$ cm.

Denoting the phase variations imposed by the phase mask on the SLM as $\varphi(x', y')$, the field can be presented as $E(x', y', z = 0) = E_0 \, \mathrm{e}^{-(x'^2+y'^2)/w_0^2} \, \mathrm{e}^{\mathrm{i}\varphi(x',y')}$, and consequently, the Fresnel diffraction integral can be written as

$$E(x, y, z = L) \cong -\frac{\mathrm{i}}{\lambda L} \, \mathrm{e}^{\mathrm{i}kL} \, \mathrm{e}^{\mathrm{i}\frac{k}{2L}(x^2+y^2)} \times \int_{-\infty}^{\infty} \mathrm{d}x' \int_{-\infty}^{\infty} \mathrm{d}y' \, E_0 \, \mathrm{e}^{-(x'^2+y'^2)/w_0^2} \times \mathrm{e}^{\mathrm{i}\frac{k}{2L}(x'^2+y'^2)} \, \mathrm{e}^{-\mathrm{i}\frac{k}{L}(x\,x'+y\,y')} \, \mathrm{e}^{\mathrm{i}\varphi(x',y')}. \quad (1)$$

Here $k = 2\pi/\lambda$ is the wave number, λ is the wavelength, and $L = 70$ cm is the propagation distance after the SLM. In the quasi-HG modes, the neighboring side lobes are out of phase by π. Since the phase factor can be factorized as $\mathrm{e}^{\mathrm{i}\varphi(x',y')} = \mathrm{e}^{\mathrm{i}\varphi_x(x')} \, \mathrm{e}^{\mathrm{i}\varphi_y(y')}$, the integrals over x and y axes were calculated independently for the phase distributions in the inset of Fig. 1a.

The validity of this approximation is determined by the conditions: $L \gg a$ and $a^4/(4\lambda L^3) \ll 1$ (a is the characteristic dimension of the beam). The latter condition requires that the quadratic terms in the phase are the dominant compared to the higher order terms that can be neglected. The Fresnel diffraction corresponding to the propagation in the near wave field is realized for $F = a^2/\lambda L \gg 1$, where F is the Fresnel number. For $F \ll 1$ the Fraunhofer diffraction and the far field wave propagation are realized. The initial beam had a radius $w_0 = 0.82$ mm, a small divergence $< 10^{-3}$ rad, and was close to normal incidence on the SLM. For the initial beam propagating from the SLM to the CCD camera, the Fresnel number is $F = 1.2$, which corresponds to the transition from the near to the far field, and the conditions of (1) validity are well fulfilled since $L = 70$ cm $\gg w_0 = 0.082$ cm and $w_0^4/(4\lambda L^3) \simeq 0.002 \ll 1$. By imposing the phase mask, even smaller spatial scale variations are introduced in the beam with characteristic dimension $a < w_0$, for which these conditions are satisfied even better.

The calculated intensity distributions are presented in Fig. 2e–h. We stress that the intensity distributions in Fig. 2f–h are calculated for phase only modification of the incident Gaussian beam at the position of the SLM. In the experiment, at sub-critical laser intensities (no filament formation), we observed similar structures of quasi-HG beams. The experimental counterparts of calculated distributions from (f–h) are shown in panels (b–d) of Fig. 2.

In the case in Fig. 2a, where there is no imposed additional phase, the beam arrives at the CCD with only a small divergence. In the case in Fig. 2b, a mask with a sharp phase step in the vertical y-direction equal to π rad is imposed, resulting in phase-edge diffraction [39], leading to the intensity oscillations in the vertical direction, while in the horizontal x-direction the diffraction is similar to the unperturbed beam. In Fig. 2c, the phase step is in the horizontal direction, so the edge-type diffraction happens in the horizontal direction. In Fig. 2d, the phase steps are both in the vertical and horizontal directions, which results in an oscillatory intensity behavior in both directions and the formation of clearly visible lobes with gradually decreasing intensity. We note that in the diffraction on a phase step, the spacing between the peaks of the lobes and the widths of the lobes is increasing with the propagation distance L from the SLM proportionally to $\sqrt{\lambda L}$ [39]. Consequently, if the distance between the SLM and the cuvette with water is changing, the intensity will vary inversely proportional to the distance, i.e, $\sim 1/z$. As is shown further, the produced structure of the intensity distribution will define the structure of the filament formation.

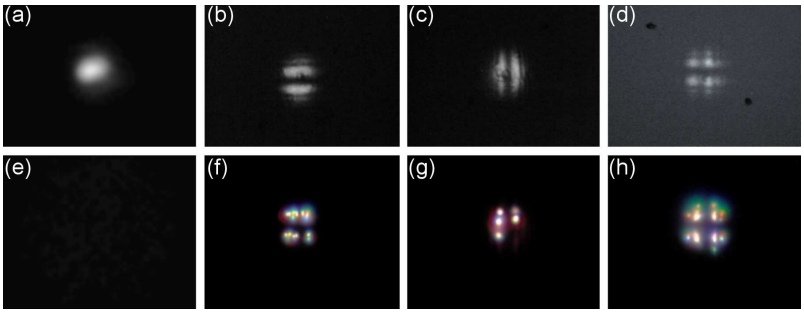

Fig. 3. The measured IR (a–d) and white-light (e–h) intensity distributions of the quasi-HG beams at the exit of the cuvette.

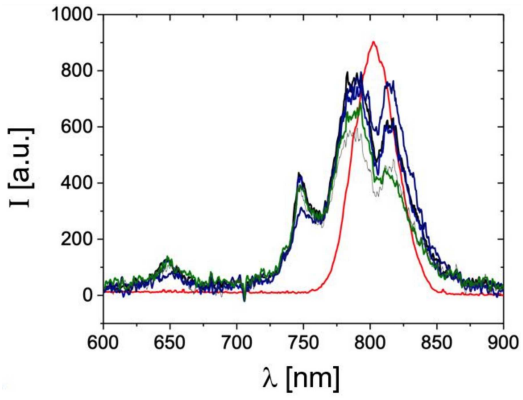

Fig. 4. The recorded spectra for the incident laser wavelength (red color) and five filaments (dark colors).

To generate filaments and related white-light supercontinuum, the quasi-HG beams were sent into a 5 cm long cuvette containing water. The laser power was adjusted to threshold power so that there was no filament generation with the incoming original Gaussian beam. Then we switched phase masks on the SLM and visualized filament generation after the water cuvette. By changing the distance between the SLM and the water cuvette, we adjusted the peak intensity in the intensity distribution lobes pattern, causing the critical threshold of filament formation to be exceeded. Then, generated white-light and incident IR radiation around 800 nm were effectively separated by reflecting the light at around 800 nm and transmitting the white-light from 400 to 700 nm with a dielectric mirror (see the transmission–reflection plot in Fig. 1b). The separated IR radiation and the generated white-light were recorded on two CCD cameras. The distributions of the filtered IR beams (light around 800nm) are presented in Fig. 3a–d. Since only a small portion of the initial beam went into the white-light generation, the observed distributions of the IR beams were quite similar to those in Fig. 2.

The generated filaments are shown in Fig. 3e–h. As seen in Fig. 3e, the incident Gaussian beam mode showed no white-light production, but the HG_{01}, HG_{10}, and HG_{11} beam modes generated individual filaments, which followed the structure of the beam lobes (Fig. 3f–h). In the experiment (and in the calculation also), we modified only the phase within the initial Gaussian beam profile because we have phase-only SLM. Thus, the resulting HG modes are expected to be superpositions of HG_{01}, HG_{10}, HG_{11}, and higher modes. It can be seen in generated HG patterns by the appearance of several side lobes. In the experiments, the filaments can be distinguished and counted. The light from the separate filaments can be also discerned. The higher intensity leads to a larger nonlinear refractive index contribution. Thus, the modified refractive index profile behaves as a focusing lens during the pulse propagation in water, which leads to self-focusing and filament formation. Filament generation occurs in our experiment at optical intensities far above the self-focusing limit, resulting in a relatively short length for the development of this process. Besides the larger-scale spatial intensity modulation due to the formation of side lobes, there are always small-scale inhomogeneities in the beam that give rise to the multiple filament formation within the lobes, provided that the intensity is sufficiently high. The number and positioning of the multiple filaments within one intensity lobe are determined by these intensity inhomogeneities, the intensity level, and such processes as the filament competition [17, 40] and the interaction of the filament core with the surrounding energy reservoir [41]. By modifying the intensity structures of the incident beam on SLM, we observed that filament generation can be controlled and organized.

In addition, the recorded spectra for initial laser beam (red color) and generated filaments (dark colors) around the central laser wavelength 800 nm are presented in Fig. 4. One observes that there is a dip formed in the vicinity of the spectral maximum (at about 800 nm) of the incident pulse and that there are new spectral components generated with shorter and longer wavelengths in the spectra corresponding to the filaments. When a femtosecond laser pulse produces filaments as a result of self-focusing, this phenomenon is accompanied by several nonlinear effects, such as self-steepening,

self-phase-modulation, and also ionization, when the intensity sufficiently increased. The spectral broadening of the incoming pulse that covers the visible part of the spectrum is perceived as a white-light generation and presents a broad spectral continuum. What is also important, the positions and characteristics of the filaments produced in each experimentally created configuration of quasi-HG modes are highly reproducible, thus overcoming the limitations in the arrangement of well-defined filament structures set by a somewhat noisy profile of the laser beam.

3. Conclusion

We report the results of the experiment on controlling and organizing femtosecond laser filamentation and the white-light generation in water by forming different transverse intensity structures of the incident beam. By creating quasi-HG beam modes from the initial Gaussian beam, we have shown that the structure of filaments and the related white-light formation can be predetermined by the beam mode structure. The filaments are distinguishable and countable since the light produced by the separate filaments can be clearly discerned. In the experimental settings, there was only one incident beam, so the light sources produced by the side lobes were mutually coherent. This coherence is an important property for realizing pump-probe spectroscopy and other experiments. By using the flexibility of phase masks on the SLM, beam modes can be created with desired intensity profiles, thus opening the possibility of creating and controlling well-defined filament structures that can be used in various applications.

Acknowledgments

This work was partially supported by Çanakkale Onsekiz Mart University, The Scientific Research Coordination Unit, Project number: FBA-2021-3488, and the Robert A. Welch Foundation Grant No. A1546.

References

[1] R.W. Boyd, S.G. Lukishova, Y.R. Shen, *Self-focusing: Past and Present: Fundamentals and Prospects*, Springer, New York, USA 2009.

[2] S.L. Chin, S.A. Hosseini, W. Liu, Q. Luo, F. Théberge, N. Aközbek, A. Becker, V.P. Kandidov, O.G. Kosareva, H. Schroeder, *Can. J. Phys.* **83**, 863 (2005).

[3] A. Couairon, A. Mysyrowicz, *Phys. Rep.* **441**, 47 (2007).

[4] M. Vengris, N. Garejev, G. Tamošauskas, A. Čepėnas, L. Rimkus, A. Varanavičius, V. Jukna, A. Dubietis, *Sci. Rep.* **9**, 9011 (2019).

[5] A. Dubietis, G. Tamošauskas, R. Šuminas, V. Jukna, A. Couairon, *Lith. J. Phys* **57**, 3 (2017).

[6] Q. Luo, H.L. Xu, S.A. Hosseini, J.F. Daigle, F. Théberge, M. Sharifi, S.L. Chin, *Appl. Phys. B* **82**, 105 (2006).

[7] H.L. Xu, S.L. Chin, *Sensors* **11**, 32 (2011).

[8] J. Kasparian, M. Rodriguez, G. Méjean et al., *Science* **301**, 61 (2003).

[9] F. Krausz, M. Ivanov, *Rev. Mod. Phys.* **81**, 163 (2009).

[10] P. Agostini, L. F. DiMauro, *Rep. Prog. Phys.* **67**, 813 (2004).

[11] E. Goulielmakis, M. Schultze, M. Hofstetter et al., *Science* **320**, 1614 (2008).

[12] S.L. Chin, W. Liu, F. Théberge, Q. Luo, S.A. Hosseini, V.P. Kandidov, O.G. Kosareva, N. Aközbek, A. Becker, H. Schroeder, *Some Fundamental Concepts of Femtosecond Laser Filamentation*, in: *Progress in Ultrafast Intense Laser Science III*, Eds. K. Yamanouchi, S.L. Chin, P. Agostini, G. Ferrante, Springer, Berlin 2008.

[13] L. Bergé, S. Skupin, R. Nuter, J. Kasparian, J.P. Wolf, *Rep. Prog. Phys.* **70**, 1633 (2007).

[14] S.L. Chin, T.J. Wang, C. Marceau et al., *Laser Phys.* **22**, 1 (2012).

[15] J.P. Wolf, *Rep. Prog. Phys.* **81**, 026001 (2017).

[16] H. Schroeder, S.L. Chin, *Opt. Commun.* **234**, 399 (2004).

[17] S.A. Hosseini, Q. Luo, B. Ferland, W. Liu, S.L. Chin, O.G. Kosareva, N.A. Panov, N. Aközbek, V.P. Kandidov, *AIP Conf. Proc.* **748**, 198 (2005).

[18] W. Liu, S.A. Hosseini, Q. Luo, B. Ferland, S.L. Chin, O.G. Kosareva, N.A. Panov, V.P. Kandidov, *New J. Phys.* **6**, 6 (2004).

[19] G. Méchain, A. Couairon, Y.B. André, C. D'Amico, M. Franco, B. Prade, S. Tzortzakis, A. Mysyrowicz, R. Sauerbrey, *Appl. Phys. B* **79**, 379 (2004).

[20] H. Schroeder, J. Liu, S.L. Chin, *Opt. Express* **12**, 4768 (2004).

[21] A. Dubietis, G. Tamoscauskas, G. Fibich, B. Ilan, *Opt. Lett.* **29**, 1126 (2004).

[22] G. Méchain, A. Couairon, M. Franco, B. Prade, A. Mysyrowicz, *Phys. Rev. Lett.* **93**, 035003 (2004).

[23] G. Kaya, *Eur. Phys. J. D* **74**, 38 (2020).

[24] O. Mendoza-Yero, M. Carbonell-Leal, C. Doñate-Buendía, G. Mínguez-Vega, J. Lancis, *Opt. Express* **24**, 15307 (2016).

[25] V.P. Kandidov, N. Akozbek, M. Scalora, O.G. Kosareva, A.V. Nyakk, Q. Luo, S.A. Hosseini, S.L. Chin, *App. Phys. B* **80**, 267 (2005).

[26] V. Koubassov, J.F. Laprise, F. Théberge, E. Förster, R. Sauerbrey, B. Müller, U. Glatzel, S.L. Chin, *App. Phys. A* **79**, 499 (2004).

[27] V.D. Zvorykin, S.A. Goncharov, A.A. Ionin et al., *Nucl Instrum Methods Phys Res B* **402**, 331 (2017).

[28] K. Midorikawa, H. Kawano, A. Suda, C. Nagura, M. Obara, *Appl. Phys. Lett.* **80**, 923 (2002).

[29] A. Camino, Z. Hao, X. Liu, J. Lin, *Opt. Express* **21**, 7908 (2013).

[30] G. Fibich, S. Eisenmann, B. Ilan, A. Zigler, *Opt. Lett.* **29**, 1772 (2004).

[31] Z.-Q. Hao, J. Zhang, T.-T. Xi, X.-H. Yuan, Z.-Y. Zheng, X. Lu, M.-Y. Yu, Y.-T. Li, Z.-H. Wang, W. Zhao, Z.-Y. Wei, *Opt. Express* **15**, 16102 (2007).

[32] D.V. Apeksimov, Y.E. Geints, A.A. Zemlyanov, A.M. Kabanov, V.K. Oshlakov, A.V. Petrov, G.G. Matvienko, *Appl. Opt.* **57**, 9760 (2018).

[33] A.A. Ionin, N.G. Iroshnikov, O.G. Kosareva, A.V. Larichev, D.V. Mokrousova, N.A. Panov, L.V. Seleznev, D.V. Sinitsyn, E.S. Sunchugasheva, *J. Opt. Soc. Am. B* **30**, 2257 (2013).

[34] A. Owyoung, R.W. Hellwarth, N. George, *Phys. Rev. B* **5**, 628 (1972).

[35] P.P. Li, M.Q. Cai, J.Q. Lü, D. Wang, G.G. Liu, S.X. Qian, Y. Li, C. Tu, H.T. Wang, *AIP Adv.* **6**, 125103 (2016).

[36] K. Cook, R. McGeorge, A.K. Kar, M.R. Taghizadeh, R.A. Lamb, *Appl. Phys. Lett.* **86**, 021105 (2005).

[37] J. Peatross, M. Ware, *Physics of Light and Optics*, Brigham Young University, 2011.

[38] N. Kaya, J. Strohaber, A.A. Kolomenskii, G. Kaya, H. Schroeder, H.A. Schuessler, *Opt. Express* **20**, 13337 (2012).

[39] M.T. Tavassoly, H. Salvdari, *Int. j. opt. photonics* **14**, 195 (2020).

[40] P. Qi, L. Lin, Q. Su, N. Zhang, L. Sun, W. Liu, *Sci. Rep.* **7**, 10384 (2017).

[41] W. Liu, F. Théberge, E. Arévalo, J.F. Gravel, A. Becker, S.L. Chin, *Opt. Lett.* **30**, 2602 (2005).